Predictions for the synthesis of superheavy elements $Z = 119$ and 120

Fan Li, Long Zhu,* Zhi-Han Wu, Xiao-Bin Yu, Jun Su, and Chen-Chen Guo
Sino-French Institute of Nuclear Engineering and Technology, Sun Yat-sen University, Zhuhai 519082, China

(Received 19 April 2018; published 25 July 2018)

Within the framework of dinuclear system model, the synthesis of the superheavy elements (SHEs) $Z = 119$ and $Z = 120$ is investigated. The entrance channel effects on capture cross section, fusion probability, survival probability, and evaporation residue cross section are investigated. We calculate the production cross sections in 276 possible reactions (with stable projectiles of $Z = 20$–30 and targets with the half-lives longer than 20 days) and show the promising ones for the synthesizing SHEs $Z = 119$ and $Z = 120$. It is found that the systems ^{44}Ca + ^{252}Es and ^{40}Ca + ^{257}Fm are the most favorable to produce the SHEs $Z = 119$ and $Z = 120$ with maximal production cross sections (optimal incident energies) of 4.32 pb (204.27 MeV) and 1.24 pb (205.66 MeV), respectively.

DOI: 10.1103/PhysRevC.98.014618

I. INTRODUCTION

The prediction of "island of stability" leads the synthesis of superheavy nuclei (SHN) to a topic at the forefront of research in experimental nuclear physics in recent years. Until now, the synthesis of superheavy elements (SHEs) with $Z = 110$–113 by using cold-fusion reactions with lead- and bismuth-based targets [1,2] and with $Z = 113$–118 by using ^{48}Ca-induced complete fusion reactions in the neutron-evaporation channels have been reported [3–5]. A conspicuous phenomenon is that the evaporation residue cross sections (ERCS) for producing SHEs stay very weak: limited to several picobarns (1×10^{-12} barns). For the synthesis of the element Og ($Z = 118$), the ERCS maintains just $0.5^{+1.6}_{-0.3}$ pb [4]. There has been an attempt to synthesize the SHEs $Z = 120$ through reactions ^{58}Fe + ^{244}Pu [6] and ^{54}Cr + ^{248}Cm [7]. Unfortunately, no correlated decay chains were observed. These limited cross sections make the research on searching for the optimal conditions for the synthesis of SHNs of great importance.

Inspired by abundant experimental data, a lot of approaches are developed for studying mechanism of fusion evaporation reactions, such as the macroscopic dynamics model [8,9], the fusion-by-diffusion model [10–12], multidimensional Langevin-type dynamical equations [13–19], the cluster dynamical decay model [20,21], the time-dependent Hartree-Fock theory (TDHF) [22,23], and the extension time-dependent density-matrix theory (TDDM) [24], the two-step model [25], the dinuclear system model [26–35], and empirical approaches [36,37]. In Ref. [38], by analyzing uncertainty of several models, predictive limitations of the existing fusion-evaporation models are noticed. However, it is still valuable to give some systematically investigation and comparison on production cross sections among possible combinations and predict favorable ones within one specific model [39].

In this work, within the dinuclear system (DNS) model, we seek to find the favorable candidates of projectile-target combinations for the synthesis of SHEs $Z = 119$ and $Z = 120$. The article is organized as follows. In Sec. II, the details of the DNS models are described and the comparison between the calculated ERCS with the measured data is shown. The results and the discussions are in Sec. III. In Sec. IV, we make a summary of this work.

II. DESCRIPTION OF THE MODEL

In the concept of the DNS model, the process of synthesis of SHN is devided into three steps. First, two nuclei overcome Coulomb barrier and form a dinuclear system, which can be described by the capture cross section. Second, the dinuclear system fuses to a compound nucleus. In this step, the formation of the compound nucleus is hindered by the competition with the quasifission channels and we use the complete fusion probability to measure it. Finally, the excited compound nucleus, in order to reach its ground state, loses its energy by the emission of particles or γ rays, competing with the process of fission. We use the statistical model to calculate the survival probability.

We calculate the ERCS of SHN as a sum over all partial waves J [40–42]:

$$\sigma_{\mathrm{ER}}(E_{\mathrm{c.m.}}) = \frac{\pi\hbar^2}{2\mu E_{\mathrm{c.m.}}} \sum_J (2J+1) T(E_{\mathrm{c.m.}}, J) \times P_{\mathrm{CN}}(E_{\mathrm{c.m.}}, J) W_{\mathrm{sur}}(E_{\mathrm{c.m.}}, J). \quad (1)$$

In this formula, $T(E_{\mathrm{c.m.}}, J)$ is the transmission probability. It means the probability that the colliding nuclei overcome the potential barrier and form a dinuclear system [14]. $P_{\mathrm{CN}}(E_{\mathrm{c.m.}}, J)$ is the fusion probability. $W_{\mathrm{sur}}(E_{\mathrm{c.m.}}, J)$ is the survival probability of the compound nucleus after the competition between fission and neutron evaporation [43]. $E_{\mathrm{c.m.}}$ is the incident energy in the center-of-mass system.

*Corresponding author: zhulong@mail.sysu.edu.cn

A. Capture cross section

For the heavy ions fusion reactions, the transmission probability $T(E_{\rm c.m.}, B, J)$ for a determined height of Coulomb barrier B and angular momentum J can be calculated by the Hill-Wheeler formula [44]:

$$T(E_{\rm c.m.}, B, J) = \left(1 + \exp\left\{-\frac{2\pi}{\hbar\omega(J)}\left[E_{\rm c.m.} - B - \frac{\hbar^2}{2\mu R_B^2(J)}J(J+1)\right]\right\}\right)^{-1}. \quad (2)$$

In this formula, $\hbar\omega(J) = \hbar\sqrt{-\frac{1}{\mu}\frac{\partial^2 V}{\partial R^2}|_{R=R_B}}$ is the width of the parabolic Coulomb barrier and $R_B(J)$ describes a position of the barrier. The nucleus-nucleus interaction potential with quadrupole deformation can be written as [32]

$$\begin{aligned} &V(R, \beta_1, \beta_2, \theta_1, \theta_2) \\ &= \tfrac{1}{2}C_1(\beta_1 - \beta_1^0)^2 + \tfrac{1}{2}C_2(\beta_2 - \beta_2^0)^2 \\ &\quad + V_C(R, \beta_1, \beta_2, \theta_1, \theta_2) + V_N(R, \beta_1, \beta_2, \theta_1, \theta_2). \end{aligned} \quad (3)$$

Here β_1 (β_2) is the parameter of dynamical quadrupole deformation for projectile (target). β_1^0 (β_2^0) is the parameter of static deformation for projectile (target). θ_1 (θ_2) is the angle between radius vector $\vec{r}$ and the symmetry axes of statically deformed projectile (target). $C_{1,2}$ are the stiffness parameters of the nuclear surface, which are calculated with the liquid drop model [45]:

$$C_i = (\lambda - 1)\left[(\lambda + 2)R_{0,i}^2\sigma - \frac{3}{2\pi}\frac{Z_i^2 e^2}{R_{0,i}(2\lambda + 1)}\right], \quad (4)$$

where λ is the level of the dynamical deformation. Here we only consider the quadrupole deformation ($\lambda = 2$). Because the influence of shell corrections on capture cross section is weak, we ignore the contribution of shell corrections to the stiffness parameters. The Coulomb potential takes the form in Ref. [46] as

$$\begin{aligned} &V_C(R, \beta_1, \beta_2, \theta_1, \theta_2) \\ &= \frac{Z_1 Z_2 e^2}{R} + \sqrt{\frac{9}{20\pi}}\left(\frac{Z_1 Z_2 e^2}{R^3}\right)\sum_{i=1,2} R_i^2 \beta_2^{(i)} P_2(\cos\theta_i) \\ &\quad + \left(\frac{3}{7\pi}\right)\left(\frac{Z_1 Z_2 e^2}{R^3}\right)\sum_{i=1,2} R_i^2\left[\beta_2^{(i)} P_2(\cos\theta_i)\right]^2. \end{aligned}$$

The nuclear potential is calculated by the double-folding method [47]

$$\begin{aligned} V_N(R) = C_0\Bigg\{&\frac{F_{\rm in} - F_{\rm ex}}{\rho_0}\Bigg[\int \rho_1^2(\mathbf{r})\rho_2(\mathbf{r} - \mathbf{R})d\mathbf{r} \\ &+ \int \rho_1(\mathbf{r})\rho_2^2(\mathbf{r} - \mathbf{R})d\mathbf{r} \\ &+ F_{\rm ex}\int \rho_1(\mathbf{r})\rho_2(\mathbf{r} - \mathbf{R})d\mathbf{r}\Bigg]\Bigg\} \end{aligned} \quad (5)$$

with

$$F_{\rm in,ex} = f_{\rm in,ex} + f'_{\rm in,ex}\frac{N_1 - Z_1}{A_1}\frac{N_2 - Z_2}{A_2}. \quad (6)$$

Here $C_0 = 300$ MeV fm^3, $f_{\rm in} = 0.09$, $f_{\rm ex} = -2.59$, $f'_{\rm in} = 0.42$, $f'_{\rm ex} = 0.54$. Z_1 (N_1) and Z_2 (N_2) are the proton (neutron) number of light and heavy fragments, respectively. The nuclear density distribution functions ρ_1 and ρ_2 are chosen as two parameters of Woods-Saxon types:

$$\rho_1(\mathbf{r}) = \frac{\rho_0}{1 + \exp\{[\mathbf{r} - \Re_1(\theta_1)]/a_1\}} \quad (7)$$

and

$$\rho_2(\mathbf{r} - \mathbf{R}) = \frac{\rho_0}{1 + \exp\{[|\mathbf{r} - \mathbf{R}| - \Re_2(\theta_2)]/a_2\}}. \quad (8)$$

Here $\rho_0 = 0.16$ fm^{-3}. $\Re_i = R_i[1 + \beta_i Y_{20}(\theta_i)]$ is the surface radii of the collision nuclei. β_i and R_i are quadrupole deformation parameter and the spherical radius of the ith nucleus, respectively. The diffuseness parameter equals 0.6 fm. $\mathbf{R}$ is the distance between the centers of two fragments.

According to the coupled-channels model, coupling between relative motion and other intrinsic degrees of freedom, which results in a barrier distribution rather than one single barrier, can improve the description of sub-barrier cross sections. In the reactions involving strongly deformed nucleus, the fusion barrier distributions are dominated by deformation effects [48]. The height of Coulomb barrier strongly depends on the collision orientation. Considering the barrier distribution instead of single barrier, the transmission probability can be written as [49]:

$$T(E_{\rm c.m.}, J) = \int f(B)T(E_{\rm c.m.}, B, J)\, dB, \quad (9)$$

$f(B)$ is a distribution function which is taken as the asymmetric Gaussian form:

$$f(B) = \frac{1}{N}\exp\left[-\left(\frac{B - B_m}{\Delta_{1,2}}\right)^2\right]. \quad (10)$$

Here $B_m = \frac{B_s + B_0}{2}$. B_0 is the height of the Coulomb barrier at waist-to-waist orientation ($\theta = 90^\circ$, with $\beta_1 = \beta_1^0$ and $\beta_2 = \beta_2^0$), and B_s is the minimum height of the Coulomb barrier with variance of dynamical deformation β_1 and β_2, which is determined by the same method in Ref. [32]. The widths of the asymmetric Gaussian form is $\Delta_1 = 4.5$ (for $B < B_m$) and $\Delta_2 = \frac{B_0 - B_s}{4}$ (for $B > B_m$). $N = \frac{\sqrt{\pi}(\Delta_1 + \Delta_2)}{2}$ is the normalization constant to make $f(B)$ satisfy $\int f(B)dB = 1$.

B. Complete fusion probability

We can calculate the fusion probability in the DNS model, which describes the fusion process as a diffusion process by numerically solving a set of master equations in the potential energy surface (PES). The time evolution of the distribution probability function $P(Z_1, N_1, E_1, t)$ to find fragment 1 with proton number Z_1 and neutron number N_1 in the corresponding local excitation energy E_1 is described by the following master

equation:

$$\begin{aligned}\frac{dP(Z_1,N_1,E_1,t)}{dt}&=\sum_{Z_1'}W_{Z_1,N_1;Z_1',N_1}(t)\big[d_{Z_1,N_1}P(Z_1',N_1,E_1,t)\\&-d_{Z_1',N_1}P(Z_1,N_1,E_1,t)\big]\\&+\sum_{N_1'}W_{Z_1,N_1;Z_1,N_1'}(t)\big[d_{Z_1,N_1}P(Z_1,N_1',E_1,t)\\&-d_{Z_1,N_1'}P(Z_1,N_1,E_1,t)\big]\\&-\{\Lambda^{\rm qf}[\Theta(t)]+\Lambda^{\rm fis}[\Theta(t)]\}P(Z_1,N_1,E_1,t).\end{aligned}\tag{11}$$

Here $W_{Z_1,N_1;Z_1',N_1}$ is the mean transition probability from the channel (Z_1, N_1) to (Z_1', N_1), which can be seen in Ref. [50]. d_{N_1,Z_1} denotes the microscopic dimension corresponding to the macroscopic state (Z_1, N_1). All the possible proton and neutron numbers of the fragment 1 is taken into the sum, but only one nucleon transfer is considered in the model ($N_1' = N_1 \pm 1$ and $Z_1' = Z_1 \pm 1$). The evolution of the DNS along the relative distance R leads to quasifission of the DNS. The quasifission rate $\Lambda^{\rm qf}$ can be calculated by the one-dimensional Kramers rate [51].

The excitation energy E_1 is determined by the dissipation energy from the relative motion and the PES of the DNS. The PES is defined as:

$$\begin{aligned}U(Z_1,N_1;Z_2,N_2,R)&=E_B(Z_1,N_1)+E_B(Z_2,N_2)\\&-E_B(Z,N)+V_C(R)+V_N(R),\end{aligned}\tag{12}$$

where $Z = Z_1 + Z_2$ and $N = N_1 + N_2$. $E_B(Z_i, N_i)$ and $E_B(Z, N)$ are the binding energies of the fragment i and the compound nucleus, respectively. In the DNS concept, the nucleon transfer process takes place at the bottom of the potential pocket, which permit us to consider only the mass asymmetry degree of freedom of the PES, which is defined as $\eta = (A_P - A_T)/(A_P + A_T)$.

The compound nuclear formation probability $P_{\rm CN}$ is expressed as follows:

$$P_{\rm CN}(E_{\rm c.m.},J)=\sum_{Z_1=1}^{Z_{\rm BG}}\sum_{N_1=1}^{N_{\rm BG}}P(Z_1,N_1,E_1,\tau_{\rm int}).\tag{13}$$

$Z_{\rm BG}$ and $N_{\rm BG}$ are the charge number and neutron number at the Businaro-Gallone (BG) point.

C. Survival probability

The excited compound nucleus usually emits the light particles and γ rays for its de-excitation. For synthesis of SHN, we only consider the competition between the fission and the neutron evaporation [32]. The survival probability of emitting x neutrons can be written as:

$$\begin{aligned}&W_{\rm sur}(E^*_{\rm CN},x,J)\\&=P(E^*_{\rm CN},x,J)\prod_{i=1}^{x}\left[\frac{\Gamma_n(E_i^*,J)}{\Gamma_n(E_i^*,J)+\Gamma_f(E_i^*,J)}\right].\end{aligned}\tag{14}$$

In this formula, $E^*_{\rm CN}$ denotes the excitation energy of compound nuclei, which can be calculated by $E^*_{\rm CN} = E_{\rm c.m.} + Q$, where Q is the reaction energy defined as $Q = M(P)c^2 + M(T)c^2 - M(C)c^2$. Here $M(P)$, $M(T)$, and $M(C)$ are the masses of the projectile, the target, and the compound nucleus, respectively. J is the spin of the compound nucleus, E_i^* is the excitation energy before evaporation of the ith neutron, which can be calculated by $E^*_{i+1} = E_i^* - B_i^n - 2T_i$ with the initial condition $E_1^* = E^*_{\rm CN}$. B_i^n is the separation energy of the ith neutron. $P(E^*_{\rm CN}, x, J)$ is the realization probability of evaporating x neutrons [52].

Thus, the fission decay width can be calculated by the Bohr-Wheeler transition-state method [53]:

$$\begin{aligned}\Gamma_f(E^*,J)&=\frac{1}{2\pi\rho_f(E^*,J)}\\&\times\int_{I_f}\frac{\rho_f(E^*-B_f-E_{\rm rot}-\varepsilon,J)\,d\varepsilon}{1+\exp[-2\pi(E^*-B_f-E_{\rm rot}-\varepsilon)/\hbar\omega]},\end{aligned}\tag{15}$$

where $I_f = [0, E^* - B_f - E_{\rm rot} - \delta - \frac{1}{a_f}]$.

The partial decay widths of the compound nucleus for the evaporation of the light particles can be estimated by Weisskopf-Ewing theory [54]:

$$\begin{aligned}\Gamma_\nu(E^*,J)&=\frac{(2s_\nu+1)m_\nu}{\pi^2\hbar^2\rho(E^*,J)}\int_{I_\nu}\varepsilon\rho(E^*-B_\nu\\&-E_{\rm rot}-\varepsilon,J)\sigma_{\rm inv}(\varepsilon)\,d\varepsilon,\end{aligned}\tag{16}$$

where $I_\nu = [0, E^* - B_\nu - E_{\rm rot} - \delta - \frac{1}{a}]$. Here $\sigma_{\rm inv}$ is the inverse reaction cross section for particle ν with channel energy ε [55]. $\delta = 0$, Δ, and 2Δ for odd-odd, odd-even, and even-even nuclei, respectively. $\Delta = 11/\sqrt{A}$ MeV.

D. Verification of the predictive ability of the DNS model

Up to now, the Flerov Laboratory of Nuclear Reactions of JINR in Dubna, Russia, has successfully synthesized the SHN $Z = 113$–118, which inspired us to search for the optimal conditions for synthesizing the SHEs $Z = 119$ and $Z = 120$. Figure 1 shows the comparison of the calculated ERCS with the experimental data in the reactions ^{48}Ca + ^{242}Pu [56], ^{48}Ca + ^{243}Am [57], ^{48}Ca + ^{249}Bk [58], ^{48}Ca + ^{249}Cf [4], ^{48}Ca + ^{245}Cm [4], ^{48}Ca + ^{248}Cm [56], ^{48}Ca + ^{244}Pu [59], and ^{48}Ca + ^{238}U [56]. Comparing with the measured data, the ERCS calculated by the DNS model can reproduce the experimental data within the error bar rather well. Especially for the reaction ^{48}Ca + ^{238}U, the calculated maximal ERCS in 4n channel is 2.74 pb with $E^*_{\rm CN} = 43$ MeV and that is 1.19 pb in the 3n channel with $E^*_{\rm CN} = 36$ MeV. The experimental value reaches its maximum of 2.44 pb in the 3n channel with an incident energy of 35 MeV, which is close to the calculated results. For the reaction ^{48}Ca + ^{242}Pu, the maximal ERCS in

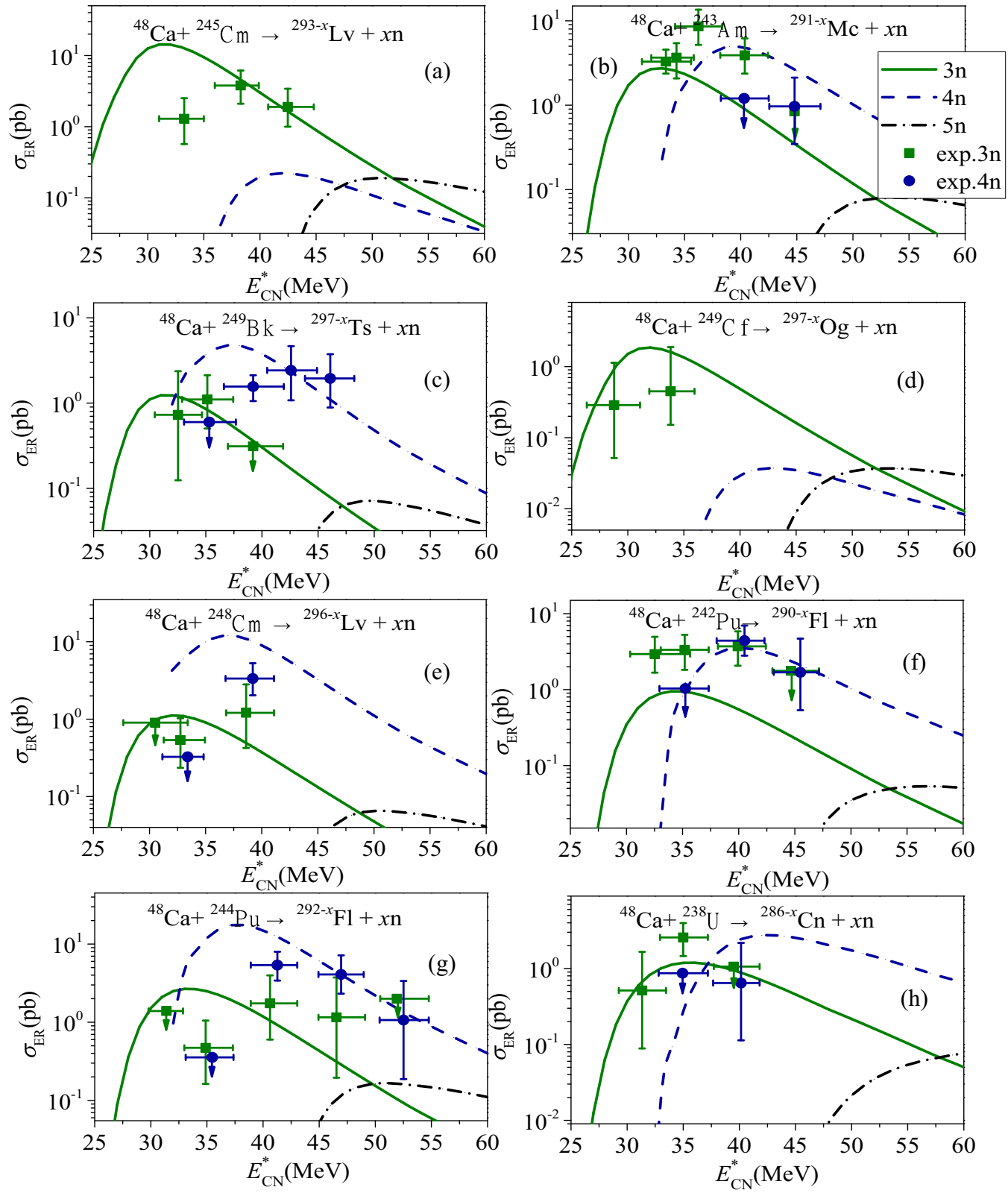

FIG. 1. Comparison of the calculated ERCS with the available experimental data for the reactions ^{48}Ca + ^{245}Cm (a), ^{48}Ca + ^{243}Am (b), ^{48}Ca + ^{249}Bk (c), ^{48}Ca + ^{249}Cf (d), ^{48}Ca + ^{248}Cm (e), ^{48}Ca + ^{242}Pu (f), ^{48}Ca + ^{244}Pu (g), and ^{48}Ca + ^{238}U (h). The calculated ERCS in the channels 3n, 4n and 5n are denoted by the green solid lines, the blue dash lines, and the black dash dot lines, respectively. The green solid squares and the blue solid circles with the error bars represent the experimental data taken from Refs. [4,56–58] for the 3n and 4n channels, respectively.

the 4n channel is 3.53 pb with $E^*_{CN} = 40.0$ MeV, which is close to the experimental cross section of 4.44 pb and incident energy of $E^*_{CN} = 41$ MeV in the 4n channel. Hence, we can conclude that this quality of agreement is acceptable that we can admit the predictive ability of the DNS model.

III. RESULTS AND DISCUSSION

Usually, the complete fusion probability increases with the increasing mass asymmetry of the system, which is defined as $\eta = (A_P - A_T)/(A_P + A_T)$, where A_P and A_T are mass numbers of projectile and target, respectively. For synthesizing the element $Z = 119$ and $Z = 120$, the combinations with stable projectiles of $Z = 20$ to 30 are studies, because of the limitation of producing a target with $Z > 100$. In this work, the candidate of targets with the half-lives more than 20 days are chosen. The entrance channel effects of hot fusion reactions are investigated. The half-lives of the nuclei are obtained from Ref. [60].

A. Synthesis of SHE $Z = 119$

For the synthesis of the SHE $Z = 119$, the reactions with ERCS more than 0.5 pb are considered as the candidates. The calculated results of these candidates are shown in Table I. In Table I, the reactions with asterisks superscript indicate the ones with the highest ERCS for the synthesis of certain isotopes of $Z = 119$. More precisely, for the synthesis of $^{291,293,295,297-299}119$, the most favorable reactions are $^{42}Ca + ^{252}Es \rightarrow {}^{291}119 + 3n$, $^{44}Ca + ^{252}Es \rightarrow {}^{293}119 + 3n$, $^{44}Ca + ^{254}Es \rightarrow {}^{295}119 + 3n$, $^{46}Ca + ^{254}Es \rightarrow {}^{297}119 + 3n$, $^{46}Ca + ^{255}Es \rightarrow {}^{298}119 + 3n$, and $^{48}Ca + ^{254}Es \rightarrow {}^{299}119 + 3n$, respectively. The predicted cross sections (incident energies) for producing $^{291,293,295,297-299}119$ are 1.71 pb (203.00 MeV), 4.32 pb (204.27 MeV), 2.13 pb (201.64 MeV), 3.60 pb (203.64 MeV), 0.61 pb (204.13 MeV), and 1.67 pb (205.96 MeV), respectively. In Table I, one can observe that the reactions ^{44}Ca (^{254}Es, 3n) and ^{50}Ti (^{248}Bk, 3n) are both leading to the compound nucleus $^{298}119$. However, for production of nucleus $^{295}119$, the ERCS of ^{44}Ca (^{254}Es, 3n) is about 2 times larger than that of ^{50}Ti (^{248}Bk, 3n). In order to clarify this phenomenon, we compare the capture cross section $\sigma_{capture}$, the complete fusion probability P_{CN} and the ERCS in the reactions $^{44}Ca + ^{254}Es$ and $^{50}Ti + ^{248}Bk$ in Fig. 2.

In Fig. 2, we notice that the capture cross section and complete fusion probability for both reactions increase with the increasing energy E^*_{CN}, which is due to the increase of probability of overcoming the Coulomb barrier and the inner fusion barrier. In Figs. 2(a) and 2(b), one can see that $\sigma_{capture}$ of the reaction $^{44}Ca + ^{254}Es$ is lower than that of the $^{50}Ti + ^{248}Bk$ in the low-E^*_{CN} region, and the ratio of $\sigma_{capture}$ between these reactions increases from 0.1 to 0.17 with the increasing E^*_{CN} from 32 to 35 MeV. Above phenomenon in capture process is due to effects of the Q value. Actually, the Coulomb barrier of the reaction $^{44}Ca + ^{254}Es$ is 188.2 MeV, which is lower than 201.6 MeV of the reaction $^{50}Ti + ^{248}Bk$. The P_{CN} in the reaction $^{44}Ca + ^{254}Es$ is much larger, and the ratio of P_{CN} maintains about 10 in the energy range of 30–40 MeV. This is mainly due to the larger mass asymmetry of the reaction $^{44}Ca + ^{254}Es$. Hence, the influence of the P_{CN} plays a significant role on ERCS. In Fig. 2(c), the ERCS of the channels 3n, 4n, and 5n for both reactions are presented. The maximal ERCS (E^*_{CN}) of the 3n channel for the reactions ^{44}Ca (^{254}Es, 3n) and ^{50}Ti (^{248}Bk, 3n) are 2.13 pb (35 MeV) and 0.69 pb (32 MeV), respectively.

Overall, for the synthesis of the SHE $Z = 119$, the projectile-target combinations listed in Table I can be taken into consideration. The maximal ERCS is 4.31 pb, reached by the reaction $^{44}Ca + ^{252}Es$ in the 3n channel with an incident

TABLE I. The calculated results for the reactions leading to the formation of $Z = 119$ with an ERCS $\geqslant 0.5$ pb.

Reaction	E^*_{CN} [a]	$E_{c.m.}$	σ_{ER} (pb)
$^{40}Ca + ^{252}Es \rightarrow {}^{289}119 + 3n$ [b]	45.0	204.08	1.27
$^{42}Ca + ^{252}Es \rightarrow {}^{291}119 + 3n$ [b]	39.0	203.00	1.71
$^{45}Sc + ^{249}Cf \rightarrow {}^{291}119 + 3n$	37.0	211.09	1.54
$^{40}Ca + ^{255}Es \rightarrow {}^{291}119 + 4n$	53.0	207.02	1.45
$^{40}Ca + ^{254}Es \rightarrow {}^{291}119 + 3n$	48.0	203.60	1.45
$^{47}Ti + ^{247}Bk \rightarrow {}^{291}119 + 3n$	37.0	219.19	1.24
$^{46}Ti + ^{248}Bk \rightarrow {}^{291}119 + 3n$	39.0	217.76	0.95
$^{51}V + ^{242}Cm \rightarrow {}^{291}119 + 2n$	27.0	225.86	0.75
$^{45}Sc + ^{248}Cf \rightarrow {}^{291}119 + 2n$	34.0	209.29	0.63
$^{52}Cr + ^{241}Am \rightarrow {}^{291}119 + 2n$	28.0	231.94	0.55
$^{44}Ca + ^{252}Es \rightarrow {}^{293}119 + 3n$ [b]	35.0	204.27	4.32
$^{43}Ca + ^{253}Es \rightarrow {}^{293}119 + 3n$	38.0	202.49	2.35
$^{42}Ca + ^{254}Es \rightarrow {}^{293}119 + 3n$	40.0	201.65	2.21
$^{45}Sc + ^{251}Cf \rightarrow {}^{293}119 + 3n$	38.0	210.03	1.68
$^{47}Ti + ^{249}Bk \rightarrow {}^{293}119 + 3n$	37.0	217.18	1.45
$^{48}Ti + ^{248}Bk \rightarrow {}^{293}119 + 3n$	34.0	219.47	1.28
$^{51}V + ^{245}Cm \rightarrow {}^{293}119 + 3n$	33.0	229.29	1.16
$^{49}Ti + ^{247}Bk \rightarrow {}^{293}119 + 3n$	34.0	222.17	1.16
$^{50}V + ^{246}Cm \rightarrow {}^{293}119 + 3n$	34.0	225.70	1.04
$^{51}V + ^{244}Cm \rightarrow {}^{293}119 + 2n$	27.0	224.00	0.98
$^{42}Ca + ^{255}Es \rightarrow {}^{293}119 + 4n$	46.0	205.95	0.97
$^{53}Cr + ^{243}Am \rightarrow {}^{293}119 + 3n$	33.0	236.20	0.95
$^{43}Ca + ^{254}Es \rightarrow {}^{293}119 + 4n$	45.0	206.90	0.64
$^{44}Ca + ^{253}Es \rightarrow {}^{293}119 + 4n$	43.0	210.94	0.56
$^{52}Cr + ^{243}Am \rightarrow {}^{293}119 + 2n$	28.0	229.49	0.51
$^{44}Ca + ^{254}Es \rightarrow {}^{295}119 + 3n$ [b]	35.0	201.64	2.13
$^{43}Ca + ^{255}Es \rightarrow {}^{295}119 + 3n$	40.0	201.49	0.94
$^{44}Ca + ^{255}Es \rightarrow {}^{295}119 + 4n$	42.0	207.59	0.86
$^{46}Ca + ^{252}Es \rightarrow {}^{295}119 + 3n$	33.0	206.00	0.77
$^{50}Ti + ^{248}Bk \rightarrow {}^{295}119 + 3n$	32.0	222.48	0.69
$^{51}V + ^{247}Cm \rightarrow {}^{295}119 + 3n$	33.0	226.83	0.66
$^{45}Sc + ^{254}Cf \rightarrow {}^{295}119 + 4n$	44.0	211.93	0.53
$^{49}Ti + ^{249}Bk \rightarrow {}^{295}119 + 3n$	33.0	218.88	0.52
$^{46}Ca + ^{254}Es \rightarrow {}^{297}119 + 3n$ [b]	32.0	203.64	3.60
$^{46}Ca + ^{255}Es \rightarrow {}^{297}119 + 4n$	39.0	210.13	2.14
$^{48}Ca + ^{252}Es \rightarrow {}^{297}119 + 3n$	31.0	208.42	1.13
$^{46}Ca + ^{255}Es \rightarrow {}^{298}119 + 3n$ [b]	33.0	204.13	0.61
$^{48}Ca + ^{254}Es \rightarrow {}^{299}119 + 3n$ [b]	29.0	205.96	1.67
$^{48}Ca + ^{255}Es \rightarrow {}^{299}119 + 4n$	36.0	212.72	1.51

[a] E^*_{CN} ($E_{c.m.}$) is the corresponding excitation energy (incident energy in the center-of-mass frame) for the maximal ER cross section in MeV.
[b] The most favorable reaction for each isotope of $Z = 119$.

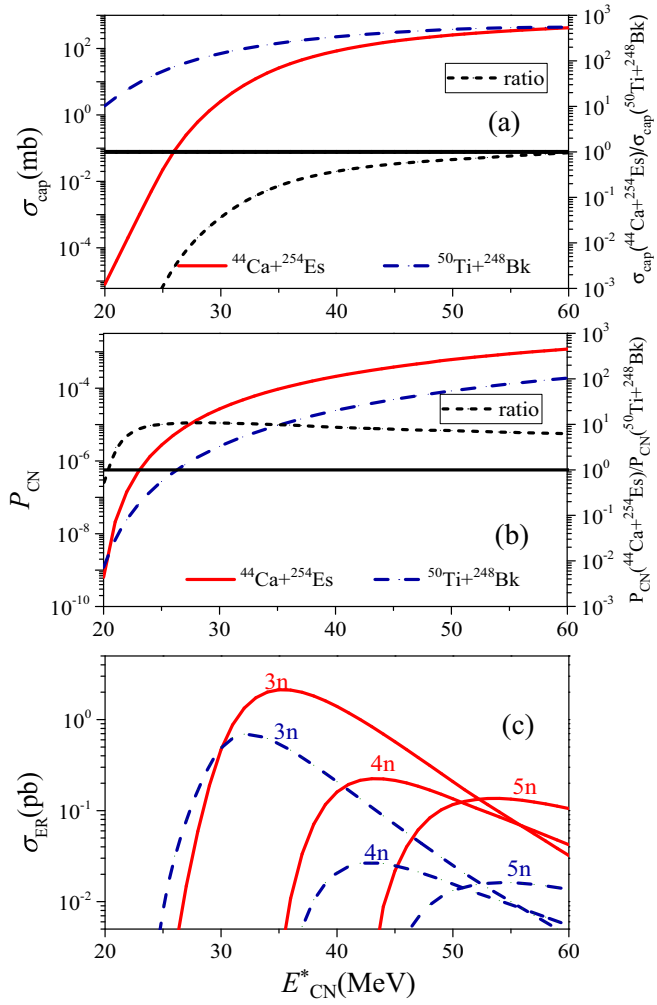

FIG. 2. (a) The calculated capture cross sections in the reactions ^{44}Ca + ^{254}Es and ^{50}Ti + ^{248}Bk, which are indicated by the red solid line and the blue dashed line, respectively. The black thin dashed line presents the ratio of $\sigma_{capture}$ (^{48}Ca + ^{254}Es) and $\sigma_{capture}$ (^{50}Ti + ^{248}Bk). The value of the ratio is shown in right side axis. The horizontal solid line denotes the value of ratio equals 1. (b) The same figure as (a) but for the complete fusion probability. (c) The calculated ERCS for the reactions ^{44}Ca(^{254}Es, xn) and ^{50}Ti(^{248}Bk, xn).

energy of 204.27 MeV. However, experimentally, Es is difficult to collect in an enough amount to produce a target sufficiently thick. So Ti isotopes can be considered as projectiles.

B. Synthesis of SHE $Z = 120$

For the synthesis of the SHE with $Z = 120$, the same method as that for synthesizing the SHE with $Z = 119$ to choose the projectile-target combinations is used. A part of our calculation results (ERCS $\geqslant$ 0.1 pb) are shown in the Table II with the asterisks indicating the most favorable reactions for producing several isotopes of $Z = 120$. More precisely, for the synthesis of $^{292-294,296,298,300,302}$120, the most favorable reactions are ^{46}Ti + ^{249}Cf $\rightarrow$ ^{292}120 + 3n, ^{40}Ca + ^{257}Fm $\rightarrow$ ^{293}120 + 4n, ^{40}Ca + ^{257}Fm $\rightarrow$ ^{294}120 + 3n, ^{42}Ca + ^{257}Fm $\rightarrow$ ^{296}120 + 3n, ^{44}Ca + ^{257}Fm $\rightarrow$ ^{298}120 + 3n, ^{46}Ca + ^{257}Fm $\rightarrow$ ^{300}120 + 3n, and ^{48}Ca + ^{257}Fm $\rightarrow$ ^{302}120 + 3n, respectively. The predicted cross sections (incident energies) for producing $^{292-294,296,298,300,302}$120 are 0.24 pb (222.89 MeV), 0.17 pb (211.66 MeV), 1.24 pb (205.66 MeV), 0.29 pb (205.29 MeV), 1.04 pb (205.27 MeV), 0.50 pb (207.84 MeV), and 0.46 pb (211.07 MeV), respectively. In Table II, one can see that the ERCS decreases with the increasing proton number of the projectile due to the influence of the mass asymmetry on the complete fusion probability, such as production of ^{294}120, which is similar to the case of the synthesis of $Z = 119$. Furthermore, one can see that the ERCS of the reaction ^{40}Ca + ^{257}Fm is about 2 times larger than that of the reaction ^{48}Ca + ^{257}Fm. It is known that the ^{48}Ca is more widely used in the experiments, which leads us to analyze the projectile neutron number dependence on synthesizing SHE with $Z = 120$.

TABLE II. The calculated results for the reactions leading to the formation of $Z = 120$ with an ERCS $\geqslant$ 0.1 pb.

Reaction	E^*_{CN} [a]	$E_{c.m.}$	σ_{ER} (pb)
^{50}Cr + ^{242}Cm $\rightarrow$ ^{290}120 + 2n[b]	31.0	234.22	0.10
^{46}Ti + ^{249}Cf $\rightarrow$ ^{292}120 + 3n[b]	39.0	222.89	0.24
^{46}Ti + ^{248}Cf $\rightarrow$ ^{292}120 + 2n	34.0	219.12	0.17
^{40}Ca + ^{257}Fm $\rightarrow$ ^{292}120 + 5n	65.0	222.66	0.11
^{40}Ca + ^{257}Fm $\rightarrow$ ^{293}120 + 4n[b]	54.0	211.66	0.17
^{40}Ca + ^{257}Fm $\rightarrow$ ^{294}120 + 3n[b]	48.0	205.66	1.24
^{46}Ti + ^{251}Cf $\rightarrow$ ^{294}120 + 3n	39.0	220.39	0.37
^{45}Sc + ^{252}Es $\rightarrow$ ^{294}120 + 3n	39.0	214.17	0.34
^{46}Ti + ^{250}Cf $\rightarrow$ ^{294}120 + 2n	36.0	218.88	0.13
^{50}V + ^{247}Bk $\rightarrow$ ^{294}120 + 3n	36.0	231.13	0.12
^{52}Cr + ^{244}Cm $\rightarrow$ ^{294}120 + 2n	28.0	234.88	0.11
^{52}Cr + ^{245}Cm $\rightarrow$ ^{294}120 + 3n	35.0	240.80	0.10
^{53}Cr + ^{243}Cm $\rightarrow$ ^{294}120 + 2n	28.0	236.02	0.10
^{50}Cr + ^{247}Cm $\rightarrow$ ^{294}120 + 3n	39.0	235.12	0.10
^{42}Ca + ^{257}Fm $\rightarrow$ ^{296}120 + 3n[b]	42.0	205.29	0.29
^{45}Sc + ^{254}Es $\rightarrow$ ^{296}120 + 3n	41.0	213.40	0.13
^{43}Ca + ^{257}Fm $\rightarrow$ ^{296}120 + 4n	47.0	210.97	0.12
^{44}Ca + ^{257}Fm $\rightarrow$ ^{298}120 + 3n[b]	36.0	205.27	1.04
^{46}Ca + ^{257}Fm $\rightarrow$ ^{300}120 + 3n[b]	33.0	207.84	0.50
^{53}Cr + ^{250}Cm $\rightarrow$ ^{300}120 + 3n	32.0	234.59	0.13
^{48}Ca + ^{257}Fm $\rightarrow$ ^{302}120 + 3n[b]	30.0	211.07	0.46

[a] $E^*_{CN}(E_{c.m.})$ is the corresponding excitation energy (incident energy in the center-of-mass frame) for the maximal ER cross section in MeV.
[b] The most favorable reaction for each isotope of $Z = 120$.

In Fig. 3, we present the capture cross sections $\sigma_{capture}$, the complete fusion probabilities P_{CN}, the survival probabilities W_{sur}, and the ERCS for the reactions ^{40}Ca + ^{257}Fm and ^{48}Ca + ^{257}Fm. In Figs. 3(a) and 3(b), we also use the black thin dashed lines to indicate the ratios of $\sigma_{capture}$ and P_{CN} between the two reactions. From Fig. 3(a), one can see that the capture cross section for the reaction ^{48}Ca + ^{257}Fm is much larger than that for ^{40}Ca + ^{257}Fm in the low-energy region, because of the Q-value effects. Neutron number of projectile strongly influences the Q value of the reaction system, as shown in Ref. [35]. However, due to larger mass asymmetry, the P_{CN} in the reaction ^{40}Ca + ^{257}Fm is two to three orders of magnitude larger than

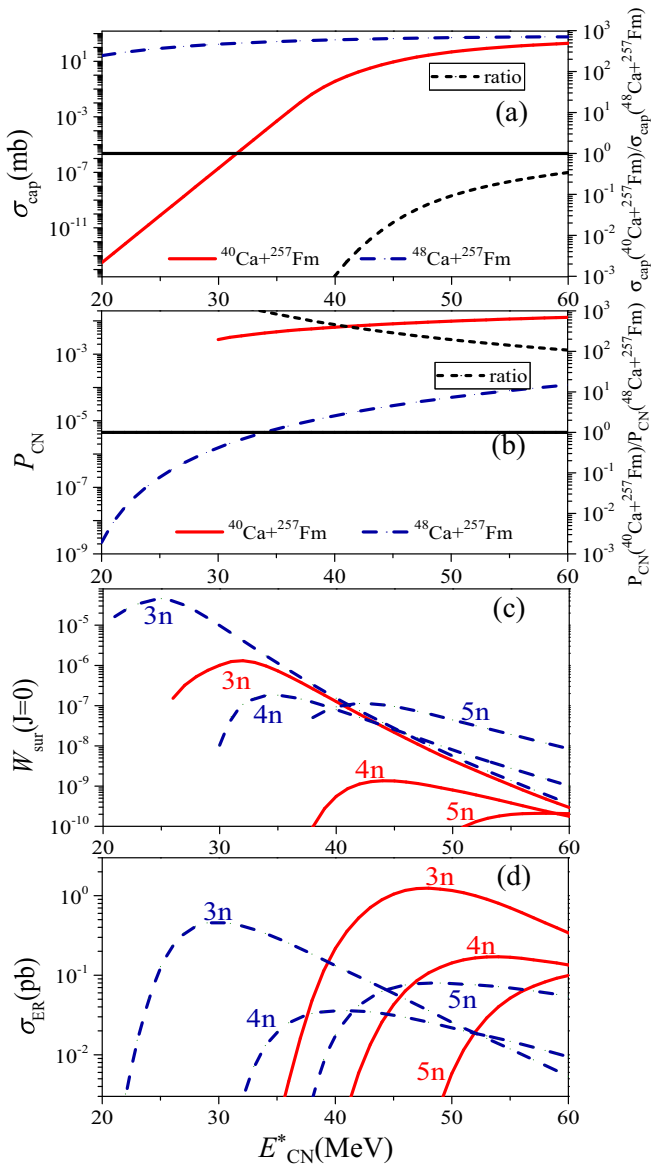

FIG. 3. (a) The same as Fig. 2(a) but for the reactions ^{40}Ca + ^{257}Fm and ^{48}Ca + ^{257}Fm. (b) The same as Fig. 2(b) but for the reactions ^{40}Ca + ^{257}Fm and ^{48}Ca + ^{257}Fm. (c) The calculated survival probabilities for the ^{297}120* and ^{305}120*. The W_{sur} for the ^{297}120* and ^{305}120* are indicated by the red solid line and the blue dash line, respectively. (d) The same as Fig. 2(c) but for the reactions ^{40}Ca + ^{257}Fm and ^{48}Ca + ^{257}Fm.

that in the reaction ^{48}Ca + ^{257}Fm from 30 to 60 MeV. As an inspection of Fig. 3(c), in low E^*_{CN} region, the survival probability of 3n channel for the reaction ^{48}Ca + ^{257}Fm is about 1 order of magnitude larger than that for the reaction ^{40}Ca + ^{257}Fm. This is because of larger neutron-richness of compound nucleus formed in the reaction ^{48}Ca + ^{257}Fm. With the increasing excitation energy the influence of neutron-richness on survival probability is weaken. The survival probability of ^{297}120* and ^{305}120* in the 3n channel are close for $E^*_{CN} \geqslant 35$ MeV. Therefore, due to much larger fusion probability, the maximal ERCS in the reaction ^{40}Ca + ^{257}Fm → ^{294}120 + 3n is larger than that in ^{48}Ca + ^{257}Fm → ^{302}120 + 3n. The maximal ERCS (E^*_{CN}) in the reaction ^{40}Ca + ^{257}Fm → ^{294}120 + 3n and ^{48}Ca + ^{257}Fm → ^{302}120 + 3n are 1.24 pb (48 MeV) and 0.46 pb (30 MeV), respectively. In comparison to the reaction ^{40}Ca + ^{257}Fm, the fusion process is a main hindrance in the reaction ^{48}Ca + ^{257}Fm for the synthesis of $Z = 120$. Hence, it is important to take the neutron number of projectile into consideration for searching the optimal projectile-target combinations.

Moreover, although ^{257}Fm has a half-time of 100.5 days, which is long enough for a target, it is still very difficult to collect enough amount of ^{257}Fm and it is rather expensive. According to Table II, the reaction ^{46}Ti + ^{251}Cf → ^{294}120 + 3n has a maximal ERCS of 0.37 pb. As a result, ^{46}Ti could also be considered as a favorable projectile.

Overall, in the sense of obtaining the largest ERCS, the most favorable reaction for synthesizing SHE $Z = 120$ is ^{40}Ca + ^{257}Fm → ^{294}120 + 3n, whose maximal ERCS is 1.24 pb with an incident energy of 205.66 MeV. Taking the experimental feasibility into consideration, the favorable projectile-target combinations for producing $Z = 120$ could also be ^{46}Ti + ^{251}Cf → ^{294}120 + 3n. The maximal ERCS (incident energies) is 0.37 pb (220.39 MeV). Although the maximum ERCS among all these reactions is just 1.24 pb, it still may be measurable in the future with the upgraded equipment such as those being designed by the MU-GSI-Giessen Collaboration [61]. On the other hand, for the heaviest element Og, the cross section for its production is just about 1 pb, and the SHE $Z = 113$ which was synthesized in the cold-fusion reaction ^{70}Zn + ^{209}Bi was observed with a cross-section value equal to some percentage of a picobarn [2]. Therefore, the reactions listed in Table II could be good references of the future experiments.

IV. CONCLUSIONS

In summary, within the DNS framework, the optimal reactions for the synthesis of the SHEs $Z = 119$ and $Z = 120$ are investigated. In order to verify the predictive ability of DNS model, the calculated ERCS are compared with the experimental data for producing $^{290-x}$Fl, $^{291-x}$Mc, $^{297-x}$Ts, $^{297-x}$Og, $^{293-x}$Lv, $^{296-x}$Lv, $^{292-x}$Fl, and $^{286-x}$CN. The calculated results can reproduce well the experimental data. For synthesizing SHEs $Z = 119$ and $Z = 120$, the projectile candidates are stable isotopes from Ca to Zn and the target candidates have half-lives longer than 20 days. The ERCS of 276 possible reactions for the synthesizing SHEs $Z = 119$ and $Z = 120$ are calculated. The entrance channel effects on capture cross section, fusion probability, survival probability, and ERCS are also investigated. Then, we proposed a series of favorable reactions for synthesizing SHEs with $Z = 119$ and 120.

In the sense of obtaining a greatest cross section, for synthesizing $Z = 119$, the most favorable reaction is ^{44}Ca + ^{252}Es → ^{293}119 + 3n. The largest cross section is 4.32 pb in the 3n channel with an incident energy of 204.27 MeV. For synthesizing $Z = 120$, the most favorable reaction is ^{40}Ca + ^{257}Fm → ^{294}120 + 3n, in which the maximal ERCS is 1.24 pb at $E_{c.m.} = 205.66$ MeV. The systematical calculations within other models would be also necessary and valuable for future experiments.

ACKNOWLEDGMENTS

This work was supported by the National Natural Science Foundation of China under Grant No. 11605296; the Natural Science Foundation of Guangdong Province, China (Grant No. 2016A030310208); and the National Natural Science Foundation of China under Grants No. 11405278 and No. 11605270.

[1] S. Hofmann and G. Münzenberg, Rev. Mod. Phys. **72**, 733 (2000).
[2] K. Morita, K. Morimoto, D. Kaji, H. Haba, K. Ozeki, Y. Kudou, T. Sumita, Y. Wakabayashi, A. Yoneda, K. Tanaka *et al.*, J. Phys. Soc. Jpn. **81**, 103201 (2012).
[3] Y. T. Oganessian, F. S. Abdullin, P. D. Bailey, D. E. Benker, M. E. Bennett, S. N. Dmitriev, J. G. Ezold, J. H. Hamilton, R. A. Henderson, M. G. Itkis *et al.*, Phys. Rev. Lett. **104**, 142502 (2010).
[4] Y. T. Oganessian, V. K. Utyonkov, Y. V. Lobanov, F. S. Abdullin, A. N. Polyakov, R. N. Sagaidak, I. V. Shirokovsky, Y. S. Tsyganov, A. A. Voinov, G. G. Gulbekian *et al.*, Phys. Rev. C **74**, 044602 (2006).
[5] Y. Oganessian, J. Phys. G: Nucl. Part. Phys. **34**, R165 (2007).
[6] Y. T. Oganessian, V. K. Utyonkov, Y. V. Lobanov, F. S. Abdullin, A. N. Polyakov, R. N. Sagaidak, I. V. Shirokovsky, Y. S. Tsyganov, A. A. Voinov, A. N. Mezentsev *et al.*, Phys. Rev. C **79**, 024603 (2009).
[7] S. Hofmann, S. Heinz, R. Mann, J. Maurer, G. Münzenberg, S. Antalic, W. Barth, H. G. Burkhard, L. Dahl, K. Eberhardt *et al.*, Eur. Phys. J. A **52**, 180 (2016).
[8] S. Bjørnholm and W. Swiatecki, Nucl. Phys. A **391**, 471 (1982).
[9] W. Swiatecki, Prog. Part. Nucl. Phys. **4**, 383 (1980).
[10] Z.-H. Liu and J.-D. Bao, Phys. Rev. C **83**, 044613 (2011).
[11] Z.-H. Liu and J.-D. Bao, Phys. Rev. C **89**, 024604 (2014).
[12] K. Siwek-Wilczyńska, T. Cap, M. Kowal, A. Sobiczewski, and J. Wilczyński, Phys. Rev. C **86**, 014611 (2012).
[13] V. Zagrebaev and W. Greiner, Nucl. Phys. A **944**, 257 (2015).
[14] V. I. Zagrebaev, Phys. Rev. C **64**, 034606 (2001).
[15] V. Zagrebaev and W. Greiner, J. Phys. G: Nucl. Part. Phys. **34**, 1 (2006).
[16] V. Zagrebaev and W. Greiner, Phys. Rev. C **78**, 034610 (2008).
[17] V. L. Litnevsky, G. I. Kosenko, and F. A. Ivanyuk, Phys. Rev. C **93**, 064606 (2016).
[18] V. L. Litnevsky, V. V. Pashkevich, G. I. Kosenko, and F. A. Ivanyuk, Phys. Rev. C **89**, 034626 (2014).
[19] V. L. Litnevsky, G. I. Kosenko, F. A. Ivanyuk, and V. V. Pashkevich, Phys. At. Nuclei **75**, 1500 (2012).
[20] K. Sandhu, M. K. Sharma, and R. K. Gupta, Phys. Rev. C **85**, 024604 (2012).
[21] S. Chopra, A. Kaur, Hemdeep, and R. K. Gupta, Phys. Rev. C **93**, 044604 (2016).
[22] A. S. Umar, V. E. Oberacker, J. A. Maruhn, and P.-G. Reinhard, Phys. Rev. C **81**, 064607 (2010).
[23] Chong Yu and Lu Guo, Sci. China Phys. Mech. Astron. **60**, 092011 (2017).
[24] M. Tohyama and A. S. Umar, Phys. Rev. C **93**, 034607 (2016).
[25] C. Shen, Y. Abe, D. Boilley, G. Kosenko, and E. Zhao, Int. J. Mod. Phys. E **17**, 66 (2008).
[26] G. Adamian, N. Antonenko, W. Scheid, and V. Volkov, Nucl. Phys. A **627**, 361 (1997).
[27] G. Adamian, N. Antonenko, W. Scheid, and V. Volkov, Nucl. Phys. A **633**, 409 (1998).
[28] J. Hong, G. Adamian, and N. Antonenko, Phys. Lett. B **764**, 42 (2017).
[29] X. J. Bao, Y. Gao, J. Q. Li, and H. F. Zhang, Phys. Rev. C **92**, 034612 (2015).
[30] X. J. Bao, Y. Gao, J. Q. Li, and H. F. Zhang, Phys. Rev. C **91**, 011603 (2015).
[31] X. J. Bao, S. Q. Guo, H. F. Zhang, and J. Q. Li, J. Phys. G: Nucl. Part. Phys. **43**, 125105 (2016).
[32] Z.-Q. Feng, G.-M. Jin, F. Fu, and J.-Q. Li, Nucl. Phys. A **771**, 50 (2006).
[33] Z.-Q. Feng, G.-M. Jin, J.-Q. Li, and W. Scheid, Phys. Rev. C **76**, 044606 (2007).
[34] L. Zhu, Z.-Q. Feng, C. Li, and F.-S. Zhang, Phys. Rev. C **90**, 014612 (2014).
[35] L. Zhu, J. Su, and F.-S. Zhang, Phys. Rev. C **93**, 064610 (2016).
[36] L. Zhu, W.-J. Xie, and F.-S. Zhang, Phys. Rev. C **89**, 024615 (2014).
[37] N. Wang, J. Tian, and W. Scheid, Phys. Rev. C **84**, 061601 (2011).
[38] H. Lü, D. Boilley, Y. Abe, and C. Shen, Phys. Rev. C **94**, 034616 (2016).
[39] Z. H. Wu, L. Zhu, F. Li, X. B. Yu, J. Su, and C. C. Guo, Phys. Rev. C **97**, 064609 (2018).
[40] W. Li, N. Wang, F. Jia, H. Xu, W. Zuo, Q. Li, E. Zhao, J. Li, and W. Scheid, J. Phys. G: Nucl. Part. Phys. **32**, 1143 (2006).
[41] N. V. Antonenko, E. A. Cherepanov, A. K. Nasirov, V. P. Permjakov, and V. V. Volkov, Phys. Rev. C **51**, 2635 (1995).
[42] N. Antonenko, E. Cherepanov, A. Nasirov, V. Permjakov, and V. Volkov, Phys. Lett. B **319**, 425 (1993).
[43] A. S. Zubov, G. G. Adamian, N. V. Antonenko, S. P. Ivanova, and W. Scheid, Phys. Rev. C **65**, 024308 (2002).
[44] D. L. Hill and J. A. Wheeler, Phys. Rev. **89**, 1102 (1953).
[45] W. D. Myers and W. J. Swiatecki, Nucl. Phys. **81**, 1 (1966).
[46] C. Y. Wong, Phys. Rev. Lett. **31**, 766 (1973).
[47] I. I. Gontchar, D. J. Hinde, M. Dasgupta, and J. O. Newton, Phys. Rev. C **69**, 024610 (2004).
[48] L. Zhu, J. Su, W. J. Xie, and F. S. Zhang, Nucl. Phys. A **915**, 90 (2013).
[49] B. Wang, K. Wen, W. J. Zhao, E. G. Zhao, and S. G. Zhou, At. Data Nucl. Data Tables **114**, 281 (2017).
[50] S. Ayik, B. Schürmann, and W. Nörenberg, Z. Phys. A **277**, 299 (1976).
[51] G. G. Adamian, N. V. Antonenko, and W. Scheid, Phys. Rev. C **68**, 034601 (2003).
[52] J. D. Jackson, Can. J. Phys. **34**, 767 (1956).
[53] N. Bohr and J. A. Wheeler, Phys. Rev. **56**, 426 (1939).
[54] V. Weisskopf, Phys. Rev. **52**, 295 (1937).
[55] M. Blann, Phys. Rev. C **21**, 1770 (1980).
[56] Y. T. Oganessian, V. K. Utyonkov, Y. V. Lobanov, F. S. Abdullin, A. N. Polyakov, I. V. Shirokovsky, Y. S. Tsyganov, G. G. Gulbekian, S. L. Bogomolov, B. N. Gikal *et al.*, Phys. Rev. C **70**, 064609 (2004).
[57] Y. T. Oganessian, F. S. Abdullin, S. N. Dmitriev, J. M. Gostic, J. H. Hamilton, R. A. Henderson, M. G. Itkis, K. J. Moody, A. N. Polyakov, A. V. Ramayya *et al.*, Phys. Rev. C **87**, 014302 (2013).

[58] Y. T. Oganessian, F. S. Abdullin, C. Alexander, J. Binder, R. A. Boll, S. N. Dmitriev, J. Ezold, K. Felker, J. M. Gostic, R. K. Grzywacz *et al.*, Phys. Rev. C **87**, 054621 (2013).

[59] Y. T. Oganessian, V. K. Utyonkov, Y. V. Lobanov, F. S. Abdullin, A. N. Polyakov, I. V. Shirokovsky, Y. S. Tsyganov, G. G. Gulbekian, S. L. Bogomolov, B. N. Gikal *et al.*, Phys. Rev. C **69**, 054607 (2004).

[60] Livechart, Table of nuclides: Nuclear structure and decay data, https://www-nds.iaea.org/relnsd/vcharthtml/VChartHTML.html.

[61] S. Heinz, W. Barth, B. Franczak, H. Geissel, M. Gupta, S. Hofmann, S. Mickat, G. Münzenberg, W. Plaß, C. Scheidenberger *et al.*, Nucl. Instrum. Methods B **317**, 354 (2013).